Journal of Inorganic Biochemistry 198 (2019) 110719

Contents lists available at ScienceDirect

Journal of Inorganic Biochemistry

journal homepage: www.elsevier.com/locate/jinorgbio

Stability of antibacterial Te(IV) compounds: A combined experimental and computational study

Kenneth D'Arcy[a], Adam Patrick Doyle[b], Kevin Kavanagh[b], Luca Ronconi[c], Barbara Fresch[d], Diego Montagner[a,*]

[a] Department of Chemistry, Maynooth University, Maynooth, Ireland
[b] Department of Biology, Maynooth University, Maynooth, Ireland
[c] School of Chemistry, National University of Ireland Galway, Galway, Ireland
[d] Department of Chemical Science, University of Padova, Italy

A B S T R A C T

Inorganic Te(IV) compounds are important cysteine protease inhibitors and antimicrobial agents; AS-101 [ammonium trichloro (dioxoethylene-O,O′)tellurate] is the first compound of a family with formula $NH_4[C_2H_4Cl_3O_2Te]$, where a Te(IV) centre is bound to a chelate ethylene glycol, and showed several protective therapeutic applications. This compound is lacking in stability performance and is subjected to hydrolysis reaction with displacement of the diol ligand. In this paper, we report the stability trend of a series of analogues complexes of AS-101 with generic formula $NH_4[(RC_2H_3O_2)Cl_3Te]$, where R is an alkyl group with different chain length and different electronic properties, in order to find a correlation between structure and stability in aqueous-physiological conditions. The stability was studied in solution *via* multinuclear NMR spectroscopy (^1H, ^{13}C, ^{125}Te) and computationally at the Density Functional Theory level with an explicit micro solvation model. The combined experimental and theoretical work highlights the essential role of the solvating environment and provides mechanistic insights into the complex decomposition reaction. Antimicrobial activity of the compounds was assessed against different bacterial strains.

1. Introduction

Tellurium is a metalloid element with several available oxidation states going from −2 to +6 [1]. Tellurides of formula M_2Te are compounds formed by Te(-II) and noble elements such as Au or Ag that are highly unstable and in the presence of oxygen's are oxidised to tellurite $[Te(IV)O_3]^{2-}$ [2]. The biological properties of tellurium are poorly characterized, but it is known that some bacteria and fungi are able to uptake Te as amino acids, replacing the Sulfur atom and forming Tellurium-cysteine and Tellurium methionine [3,4]. The oxidation state +4 is the most stable and interesting from biological application, with multiple complexes of organo-tellurium(IV), containing a direct Te—C bond, reported. These complexes are stable in aqueous solution and seem to have a promising and potential role in protease inhibition and integrin inactivation [5–14]. Besides these families of organo-tellurium complexes, Albeck and co-worker's ultimately developed two "inorganic" tellurate Te(IV) compounds, named AS-101 [ammonium trichloro (dioxoethylene-O,O′)tellurate] and SAS [octa-*O*-bis-(*R*,*R*)-tartarate ditellurane] whose structure is depicted in Fig. 1. These complexes are effective inhibitors of cysteine protease and showed several protective therapeutic applications and *in vivo*, preclinical and clinical studies have been conducted [15–26].

Te(IV) compounds can inhibit integrin functions such as adhesion, migration and metalloproteinase secretion mediation in B16F10 murine melanoma cells. AS-101 in particular, can stimulate the proliferation of normal lymphoid cells producing lymphokines that are regulators of lymphopoiesis and myelopoiesis [17]. AS-101 also showed strong antibacterial activity in particular on Gram-negative bacterium *Enterobacter cloacae* [27]. Recently, Albeck and Cunha, reported that AS-101 is not stable in physiological conditions and is subjected to hydrolysis where the diol ligand is displaced with the formation of $[Te(IV)OCl_3]^-$, which is likely the bioactive species in biological investigation [28,29]. Due to the promising activity of AS-101 in term of anticancer and immune-modulating properties, we sought to design, synthesise and characterize a series of AS-101 analogues with different ligands, in order to investigate their stability properties in aqueous environment and ultimately found a tellurate Te(IV) complex stable enough to perform biological studies in physiological conditions.

The ethylene glycol of AS-101 has been substituted with a series of diols with increasing alkyl chain length and electron withdrawing groups, producing eight novel Te(IV) complexes with formula $NH_4[(RC_2H_3O_2)Cl_3Te]$ (where R = H (**1**); CH_3 (**2**); CH_2CH_3 (**3**); $CH_2CH_2CH_3$ (**4**); $CH_2CH_2CH_2CH_3$ (**5**); $CH_2CH_2CH_2CH_2CH_2CH_3$ (**6**); CH_2Cl (**7**); Ph. (**8**)). The aqueous stability has been evaluated using ^1H, ^{13}C and ^{125}Te NMR and theoretical studies allowed an understanding of the molecular basis of the observed trend. The modelling of the reaction

* Corresponding author.
E-mail addresses: barbara.fresch@unipd.it (B. Fresch), diego.montagner@mu.ie (D. Montagner).

https://doi.org/10.1016/j.jinorgbio.2019.110719
Received 28 February 2019; Received in revised form 7 May 2019; Accepted 13 May 2019
Available online 28 May 2019

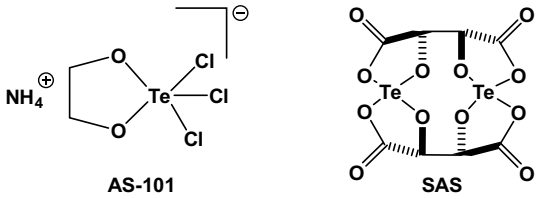

Fig. 1. Structure of the "inorganic" Te(IV) compounds AS-101 and SAS.

mechanism suggests that a longer alkyl chain substituent enhances the stability of the complex by interfering with the formation of water clusters necessary for mediating the proton transfer steps involved in the hydrolysis of the Te—O bonds. The antimicrobial activity was evaluated *in vitro* on *Escherichia coli* and other bacteria strains.

2. Experimental

2.1. Material and methods

$TeCl_4$ and all the diol ligands have been purchased from Sigma-Aldrich or TCI Europe. All solvents were used without further purification except for CH_3CN which was kept dry over molecular sieves under inert atmosphere. All NMR spectra were recorded on a Bruker Advance spectrometer with the probe at 293 K, operating at 500 MHz for the ^{1}H, at 125 MHz for the ^{13}C and at 158 MHz for the ^{125}Te nucleus, respectively. Spectra were recorded in DMSO-d_6 using Me_4Si as the internal standard for ^{1}H and ^{13}C while diphenyl ditelluride was used as external reference for ^{125}Te. All chemical shifts δ are reported in ppm. FT-IR spectra were recorded (compounds **1** and **3**) from either CsI disks (solid samples) or KRS-5 thallium bromoiodide cells (neat liquid samples) at room temperature on a Perkin Elmer Frontier FT-IR/FIR spectrophotometer in the range 4000–600 cm^{-1} (32 scans, resolution 4 cm^{-1}) and in the range 600–200 cm^{-1} (32 scans, resolution 2 cm^{-1}). Data processing was carried out using OMNIC version 5.1 (Nicolet Instrument Corporation). For all the other compounds Infrared (IR) spectra were recorded in the region 4000–400 cm^{-1} on a Perkin Elmer ATR (Attenuated Total Reflectance) precisely spectrum 100 FT/IR spectrometer. Elemental analysis (carbon, hydrogen and nitrogen) were performed with a PerkinElmer 2400 series II analyser. ESI (Electro Spray Ionisation) mass spectra were recorded in negative mode with a Waters LCT Premier XE Spectrometer. The stability of the complexes has been evaluated following the decomposition reaction by ^{1}H, ^{13}C and ^{125}Te NMR. Each compound was accurately weighted and dissolved in 400 μL of DMSO-d_6 to obtain 125 mM solution (0.05 mmoles). 10 μL of D_2O were added in three consecutive aliquots and the NMR spectra were recorded 1 h after each addition (each addition corresponds to 10 equivalents of water with respect the complex). The experiments were run in triplicate.

2.1.1. Effect of compounds on growth of E. coli

To each well of a 96-well plate (Sarstedt), 100 μL of fresh nutrient broth medium were added. A serial dilution of each compound was performed on the plate to give a concentration range of (150–0.59 μM). Cells suspension (100 μL) of *E. coli* (1 × 106 cells/mL) was added to each well and the plates were incubated at 37 °C for 24 h. The experiments were carried out in duplicate. The OD570nm of the cultures was determined using a microplate reader (Bio-Tek, Synergy HT) and all growth was expressed as a percentage of that in the control. The MIC_{50} and MIC_{80} (Minimum Inhibition Concentration) are defined as the lowest concentration to inhibit growth by 50% and 80%, respectively.

2.1.2. Computational method

Structures and energetics were modelled by Density Functional Theory (DFT) at the wB97XD/lanL2DZ level of theory, which performs well in prediction of reaction energies [30]. Implicit solvation was introduced with the *Solvation Model based on Density* (SMD) parametrization. The ground state geometry of each compound was optimized in implicit solvent by including the effect of the polarizable continuum in the self-consistent field procedure. The explicit microsolvation model was built by adding five water molecules to the reactant complex, the whole hydrated complex was then reoptimized in implicit DMSO. The initial positions of the water molecules were selected by maximizing the possibility of forming hydrogen bonds between water molecules and the compounds in order to find the most stable structures of reactants and products upon optimizations. The initial hypotheses were optimized, for the analysis we retained the three lower energy structures of the reactants (Fig. S19 in supplementary material) and the lowest energy structure of the hydrated products (Fig. S20). Frequency calculations allowed the characterization of the potential energy surface and the evaluation of the thermochemistry of the involved compounds. All computations were performed with Gaussian16 [31].

3. Results and discussion

The series of eight complexes with formula $NH_4[(RC_2H_3O_2)Cl_3Te]$ (where R = H (**1**); CH_3 (**2**); CH_2CH_3 (**3**); $CH_2CH_2CH_3$ (**4**); $CH_2CH_2CH_2CH_3$ (**5**); $CH_2CH_2CH_2CH_2CH_2CH_3$ (**6**); CH_2Cl (**7**); Ph. (**8**)), analogues of AS-101, have been synthesised as described in the Experimental part and in Scheme 1. Briefly, $TeCl_4$ and the correspondent diol were mixed in dry acetonitrile and the mixture was refluxed for several hours. The solids were collected by filtration after concentration of the CH_3CN solution or by addition of Et_2O. The complexes can be also synthesised by microwave as previously observed for AS-101 [32] and the reaction mechanism involves four steps as described by Sredni et al. [18]. The compounds were characterized by Elem. Analysis, IR spectroscopy, Mass spectrometry, ^{1}H, ^{13}C and ^{125}Te NMR (all the spectra are reported in the Supporting Information Figs. S1–8).

All the complexes show a unique ^{125}Te NMR peak in DMSO-d_6 around 1680 ppm, the typical region for these kind of species [33–34] and in the IR spectra is clearly visible the stretching of the ammonium counter cation at 3200 cm^{-1}. A detailed IR study in the range 4000–200 cm^{-1} was done for compounds **1** and **3**. Further insights into the coordination sphere of tellurium can be obtained by comparison with the IR spectra of the starting ethylene glycol, whose vibrations have been fully assigned previously [35,36]. For instance, in the mid-IR spectrum of compound **1** (Fig. S9) the bands associated with the –COH moieties of the diol (ν(OH) = 3400, δ_{ip}(COH) = 1424, δ_{oop}(COH) = 644 cm^{-1}) have disappeared, consistent with the coordination of the deprotonated glycol to the Te(IV) centre. The C—O stretching vibrations were detected at lower energy, in agreement with values reported for analogous derivatives [18]. New bands were recorded at 3234 ($\nu_a(NH_4^+)$) and 1408 ($\delta_a(NH_4^+)$) cm^{-1} accounting for the presence of the ammonium counterion [37]. In the far-IR region (Fig. S10), the spectrum of compound **1** appears dramatically different from that of ethylene glycol, the latter showing only one weak broad band at 520 cm^{-1} assigned to the δ(CCO) [35]. In line with the results reported by Albeck et al., [18] in the solid state the complex should present a distorted square-pyramidal geometry in which the two oxygen atoms of the deprotonated diol occupy the axial and one equatorial

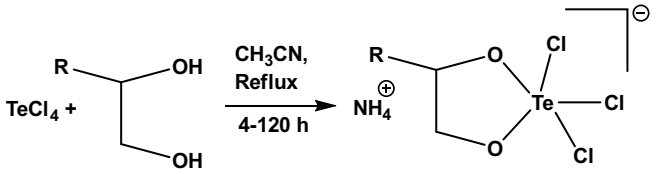

Scheme 1. Synthesis of the complexes $NH_4[(RC_2H_3O_2)Cl_3Te]$, where R = H (**1**); CH_3 (**2**); CH_2CH_3 (**3**); $CH_2CH_2CH_3$ (**4**); $CH_2CH_2CH_2CH_3$ (**5**); $CH_2CH_2CH_2CH_2CH_2CH_3$ (**6**); CH_2Cl (**7**); Ph. (**8**).

positions. Accordingly, two tellurium-oxygen stretching vibrations are foreseeable, ν(Te-O_{ax}) and ν(Te-O_{eq}), the former expected at higher frequency [38]. For **1**, Te-O vibrations were assigned to two new bands recorded at 607 and 528 cm^{-1}, respectively. Such assignments, together with the two intense bands observed at 467 and 406 cm^{-1} assigned to the overall deformation of the Te(O_2C_2)-ring, are fully consistent with those reported for analogous derivatives [39]. According to the very few relevant papers published to date, tellurium-chlorido derivatives exhibit Te—Cl stretching vibrations in the range 400–200 cm^{-1}, such as 378/312 ($TeCl_4$) [40], 220–250 ($[TeCl_6]^{2-}$) [41,42], 286/263 (Ph_2TeCl_2) [43] and 271/221 ([Te(dioxoethylene-*O,O'*)Cl_3], Raman) cm^{-1} [44]. In the present study, two new intense bands were recorded at 351 and 298 cm^{-1}, which can be reasonably assigned to the antisymmetric and symmetric stretching involving the -$TeCl_3$ moiety. The IR spectra of derivative **2** resemble closely those of **1**. The same pattern of bands was observed in the far-IR region, whereas in the 4000–600 cm^{-1} range the only minor differences would be attributed to the new vibrations involving the CH_3CH_2CH- pendant, such as those recorded at 3048 (ν(CH)), 2967/2872 ($\nu_{a,s}(CH_3)$), 1354 ($\delta_s(CH_3)$) and 776 ($\rho(CH_3)$) cm^{-1} [44]. The complexes are very stable in pure CH_3CN or DMSO solution, but they decompose upon addition of H_2O, as previously described by Albeck and co-worker's [26]. The hydrolysis reaction releases the free diol with the formation of trichloro-tellurium (IV) oxide $[TeOCl_3]^-$, as depicted in Scheme 2.

The displacement of the ligand is followed by ^1H, ^{13}C and ^{125}Te NMR (Fig. 2 for **3**): the signals of the coordinated and of the released diols appear shifted in the NMR spectra, and this effect is particularly remarked in the ^{13}C NMR for the two carbons bound to the two donor oxygen of the diols (Fig. 2 centre for compound **3** and Figs. S11–16). After addition of 10, 20 and 30 equivalents of water, as explained in the experimental part, the free diol is displaced with the formation of $NH_4[TeOCl_3]$, visible in the ^{125}Te NMR at δ 1560 ppm (Fig. 2 right). To confirm the nature of the decomposed product, 20 mg of compound **3** were dissolved in 1 mL of CH_3CN and 5 mL of H_2O and, after 2 h, the solution was dried under vacuum. The white solid obtained was washed with cold CH_3CN, H_2O and diethyl ether and further dried under high vacuum pressure. Mass spectrometry (Fig. S17, peak at (−) *m/z* 250.81 corresponding to $[Cl_3OTe]^-$) and Elem. Analysis confirm the nature of the product as $NH_4[Cl_3OTe]$ (Elem. Anal. %H (1.50), %N (5.23); found H (1.91), N (5.04)).

Analysing the integrals of the released ligand *vs* the integrals of the starting compound with respect the equivalents of water, it is possible to estimate on the stability of the complexes.

The data show that there was an evident direct proportion between the alkyl chain of the diol and the stability of the Te complexes; an increase of the chain length corresponds to an increase of the stability, with complex **6** more stable than **5**, **4**, **3**, **2** and **1** (Fig. 3). After addition of 30 eq. of water, compound **1** is almost completely decomposed while **6** is more resistant (55% not decomposed). Complex **7** with a Cl electro-withdrawing substituent is the least stable (it completely decomposes upon addition of 20 eq. of H_2O) while, unfortunately, it was not possible to evaluate the stability of complex **8**, since it was not obtained pure.

To gain a molecular understanding of the factors affecting the stability of the complexes we modelled at the quantum mechanical level complex **1** and complex **5**, representing the limiting case of short and long alkyl-chain substituent, respectively, and complex **7** with the chloro-methyl substituent. The optimized equilibrium geometries and the analysis of the electronic structures in terms of atomic charges [45,46] are reported in Fig. S18. Both atomic charges and structural parameters of the Te centre are not significantly affected by the change in the alkyl chain length nor by the chlorination of the substituent, therefore it can be concluded that the origin of the slightly different stability of the complexes does not stem from different strengths of the Te—O bonds. As it also emerges from the stability studies, the solvating environment plays a central role in establishing the equilibrium of the decomposition reaction of the complexes. Computationally, there are several approaches to treat solvation and we will use two of them in the following to elucidate the energetics of the complex decomposition. In the first approach (*implicit solvation*), the solvent is treated as a continuous, uniform dielectric medium characterized by its dielectric constant Ɛ. The solute molecules are placed inside an empty cavity within the dielectric medium and the interactions between solvent and solute consists primarily of electrostatic interactions, that is the mutual polarization of the solute and the solvent. We use the Solvation Model based on Density (SMD) which was found to perform well for predicting reaction energies in solution [47]. The reaction free energy, ΔG_r, obtained for the decomposition of the three complexes, **1**, **5** and **7**, by considering the free energy of reactants and products implicitly solvated in acetonitrile, DMSO and water are reported in Table 1, together with the free energy of the same reactions in gas-phase. Positive values of free energy of reactions reflect a stable complex which does not undergo significant decomposition. From the analysis of the values of the reaction free energy in implicit solvent we can draw two main conclusions:

i) We do see consistent trend in how the relative gas-phase stability of the three complexes is changed by solvation. Complex **5** is less prone to decomposition than complex **1** in all the considered solvents and complex **7** is the most destabilized by solvation. This can be understood by considering the solvation energies of the different species involved in the reactions (see Table S1 in the Supporting Information file) which show that the chloro-methyl substituted glycol is considerably more stabilized by solvation than the corresponding reactant complex. A word of caution must be given since the calculated difference in the reaction free energies between complex **1** and **5** ($\Delta\Delta G_r$ of about 1–1.3 kcal/mol) is small and falls within the error of the numerical method. On the other hand, such a small difference is consistent with the experimental results which report a decomposition of 0.8% for **1** and 0.4% for **5** in the case of 10 eq. of water (Fig. 3), corresponding to a difference in the reaction free energies of the two complexes of about 2 kcal/mol.

ii) Because of the active involvement of water molecules in the decomposition reaction, the implicit solvent calculations fail to predict the spontaneous decomposition of the reactants in water. Indeed, the use of a cavity model assumes that the solute electron density is not changed by specific interactions with individual solvent molecules and the reaction does not itself involve specific solvent molecules. The limitations resulting from these assumptions can be addressed by including explicit solvent molecules inside the cavity. We introduce an explicit micro-solvation environment by considering the complexes interacting with five water molecules (see the reactants in Fig. 4). The solute and its hydration shell are then considered solvated in DMSO with the implicit model to better reproduce the experimental condition of the NMR experiments. Multiple equilibrium geometries of reactants and products were

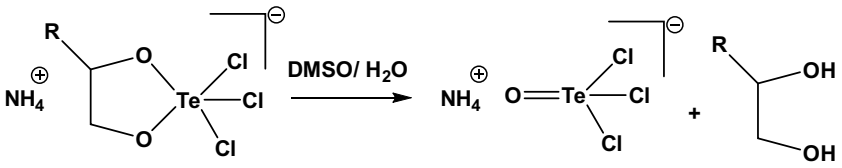

Scheme 2. Hydrolysis reaction of Te(IV) complexes

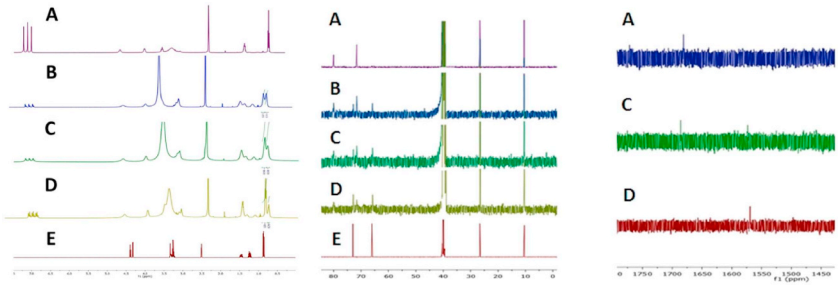

Fig. 2. ^{1}H (left), ^{13}C (centre) and ^{125}Te (right) NMR of: A) **3** (125 mM in 400 µL DMSO-d_6); B) **3** + 10 µL D_2O (10 eq.); C) **3** + 20 µL D_2O (20 eq.); D) **3** + 30 µL D_2O (20 eq.); E) free 1,2-butandiol ligand.

generated. We reported in Figs. S19 and S20 the structures of the three lower lying energy structures of the hydrated complex and the most stable structure of the products resulting from the decomposition of Compound **1**, **5** and **7**. The reaction free energies are reported in Table 1 for the different conformers of the reactants R1–R3 (Fig. S20). We recover the spontaneous decomposition of the complexes and an increased stability of the complex substituted with the longer alkyl chain in good agreement with the experimental findings. By defining the solvation contribution to the free energy of reaction as the difference between the ΔG_r calculated with the explicit micro-solvation shell model and its gas-phase value we find that these contributions are −27.3 kcal/mol, −18.2 kcal/mol and −12.6 kcal/mol for complex **7**, complex **1** and complex **5**, respectively. These results suggest that the trend in the stability of the complexes increasing with the length of the alkyl chain results from a less efficient hydration of the structure of the reactants relative to the decomposition products.

Indeed, the mechanism of the decomposition reaction involves multiple steps of proton transfer requiring the active involvement of clusters of water molecules. Mechanistic insights into the decomposition reaction are shown in Fig. 4 and they were obtained by investigating the reaction path starting from the most stable structure of the hydrated compound **1** (Reactant in Fig. 4). Structures with real frequencies corresponds to minima of the potential energy surface, that are equilibrium geometries of reactants, products and reaction intermediates. Geometries of transition states correspond to a saddle point of the Potential Energy Surface (PES) and are characterized by an imaginary frequency for the mode identifying the reaction coordinate. The mechanism of the decomposition reaction was assumed to consist of two subsequent hydrolysis steps. We identify a transition state (*TS1* in Fig. 4) corresponding to the rupture of the first Te—O bond at a free energy of +17.2 kcal/mol from the reactant complex. Breaking this bond requires both a nucleophilic attack of a water molecule to the Te centre together with a proton transfer from the water to the forming glycol molecule. Following the intrinsic reaction coordinate corresponding to the imaginary frequency of TS1 (see TS1.gif animation in the Supporting Information) we find a reaction intermediate where a -OH group is coordinated to the Te centre at an angle of about 120° from the plane of the -$TeCl_3$ moiety (*H1a* in Fig. 4). This structure can rearrange in other conformers (*H1b* and *H1c* in Fig. 4) where the most stable (+1.7 kcal/mol from the reactant) is characterized by the -OH group coordinated to Te in equatorial position. The hydrolysis of the second Te—O bond to form the free glycol molecules again requires the coordination of a second water molecule to the Te centre. This second nucleophilic attack to the Te centre comes most probably from the side opposite to the Te—O bond to break (see structure *preH2* in Fig. 4). This geometry implies that the water molecule attacking the Te centre transfers its protons to other acceptors and the protonation of the glycol is operated by a separate species (which might be a second water molecule or even a H_3O^+ ion). Most probably there are many possible paths for these multiple proton transfer steps and the mechanistic details depends on the relative position of the hydrating water molecules. The increasing of the decomposition ratio with the numbers of water equivalents observed experimentally is readily explained by considering that clusters formed by a higher number of water molecules are more efficient in mediating proton transfer steps trough the more extended H-bond network. From the intermediate structure where two -OH groups are coordinated to the Te centre (*H2* in Fig. 4) a further proton transfer step leads to the formation of the trichloro Tellurium (IV) oxide $[OCl_3Te]^-$ (*Products* in Fig. 4) where one of the vertexes of the square pyramid is occupied by a coordinated water molecule, at least in solution. In the mass spectrum of the decomposed product, as described before, the coordinated water molecule is not visible due to the ESI conditions.

Since AS-101 and Te(IV) species showed antimicrobial activity against *Enterobacter cloacae* and *Pseudomonas aeruginosa*, [27,48–51] some of the complexes synthesised, (**3**, **4** and **5**) together with the free ligands, were selected and screened for antimicrobial activity against a series of bacteria, including *Escherichia coli*, *Staphylococcus aureus*, methicillin resistant *Staphylococcus aureus* (MRSA), *Pseudomonas aeruginosa*, and the yeast *Candida albicans*.

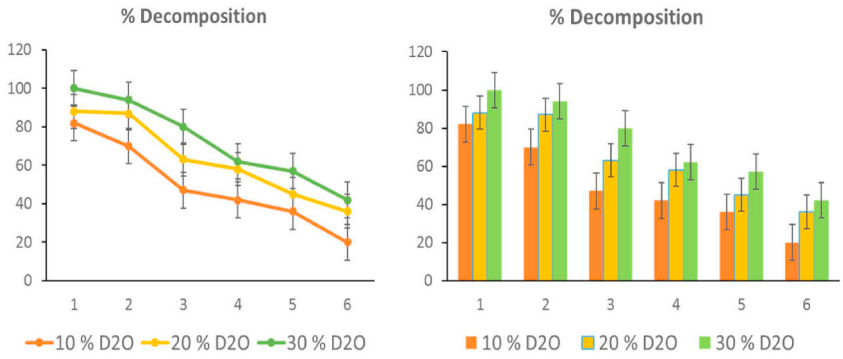

Fig. 3. Decomposition of complexes **1–6** with addition of water. Left, marked line representation; right, 2D column representation.

Table 1
Free energy of the decomposition reaction of compounds **1**, **5** and **7**. The table reports the gas-phase energy and the set of energies calculated with an implicit solvent model of acetonitrile, dimethyl sulfoxide (DMSO) and water. The reaction considered in gas-phase and in implicit solvent was $[(RC_2H_3O_2)Cl_3Te]^- + H_2O = [RC_2H_3(OH)_2] + [Cl_3OTe]^-$ where reactants and products were considered as non-interacting molecules each species was solvated separately. The second set of energies are calculated by explicit consideration of a hydration shell composed of five water molecules. The labels R1, R2 and R3 refers to three different conformers of the hydrated reactant differing by the positions of the water molecules, see Figs. S19 and S20 for the structures of reactants and products.

ΔG_r (kcal/mol)	Gas phase	Implicit solvation			Explicit microsolvation shell		
		Acetonitrile (ε = 35.688)	DMSO (ε = 46.826)	Water (ε = 78.3553)	R1	R2	R3
1	16.6	18.4	18.1	16.0	−1.6	−4.7	−5.4
5	17.5	19.4	19.4	17.2	4.9	−1.3	−2.8
7	23.3	18.2	17.9	15.9	−4.0	−11.5	−13.5

The compounds showed interesting activity against the Gram negative bacterium *E. coli* (MIC_{50} values between 15 and 20 μM as reported in Table 2) while they were less active or inactive against the other bacteria and *C. albicans*. The free diol ligands that are displaced in physiological conditions, have been analysed and they do not show any activity. We conclude that the similar activity of the complexes is probably due to the hydrolysed product $[Cl_3OTe]^-$. Interesting, a black metallic, granular layer was visible in the assay medium of *E. coli* treated plates and it is probably due to the reduction of the Te(IV) by the bacteria, as already observed by Yang and co-workers (Fig. 5) [48].

Table 2
MIC_{50} and MIC_{80} values of the compounds **3–5** in *E. coli*.

Compound	MIC_{50} (μM)	MIC_{80} (μM)
3	19.8 ± 0.5	40.5 ± 0.6
4	18.4 ± 0.4	37.8 ± 0.7
5	17.1 ± 0.6	35.7 ± 0.8

4. Conclusions

A series of Te(IV) compounds of formula $NH_4[(RC_2H_3O_2)Cl_3Te]$ where R is an alkyl chain with different length and electronic substituents, was synthesised and fully characterized and the stability in aqueous media was investigated. Experimental observations are matching with theoretical modelling using the explicit micro solvation method, showing that all the complexes release the diol ligand upon addition of water with hydrolytic cleavage of the Te—O bonds. The decomposition reaction consists in two subsequent hydrolysis steps and compounds with longer chains are more stable because the alkyl group causes a less efficient hydration of the products and hinders the necessary proton transfer steps in the reaction. Nevertheless, even if there is a correlation between alkyl chain length and stability, this latter is not enough to claim that the promising antimicrobial activity observed, in particular against Gram negative *E. coli* bacteria, is due to the starting compounds. We can conclude instead, that these compounds act as prodrugs by realising the hydrolysed product $NH_4[Cl_3OTe]$, which acts as the real bioactive species.

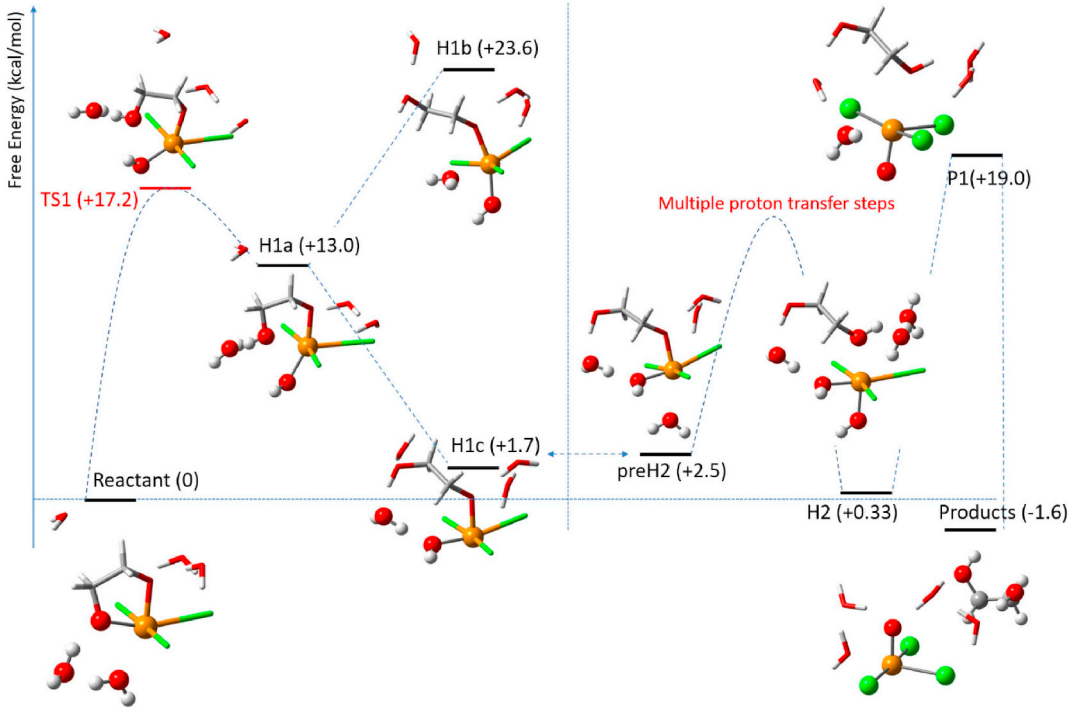

Fig. 4. Mechanistic insights into the decomposition reaction of **1** by considering an explicit micro-solvation shell formed by 5 molecules of water. The free energy of the structures relative to the reactant complex is reported in parenthesis (in unit of kcal/mol). Geometries corresponding to black lines are minima of the potential energy surface while TS1 is a transition state with an imaginary frequency of 131 cm^{-1} (see TS1.gif in SI). The vertical line in the middle of the picture divides the hydrolysis of the fist Te—O bond from the hydrolysis of the second Te—O bond which leads to the formation of the free glycol.

Fig. 5. Black precipitate observed at the bottom of the plate of *E. coli* treated with **3**.

Supplementary data to this article can be found online at https://doi.org/10.1016/j.jinorgbio.2019.110719.

Acknowledgments

KDA is grateful to INTEL for sponsoring the M.Sc. scholarship. BF acknowledges the support of the Italian Ministero dell'Istruzione, Università e Ricerca through the grant Rita Levi Montalcini (2013).

Declaration of competing interest

The authors declare no conflict of interest.

References

[1] I. Haiduc, R.B. King, M.G. Newton, Chem. Rev. 94 (1994) 301–326.
[2] M. Ruck, F. Locherer, Coord. Chem. Rev. 285 (2015) 1–10.
[3] S.E. Ramadan, A.A. Razak, A.M. Ragab, M. El-Meleigy, Biol. Trace Elem. Res. 20 (1988) 225–232.
[4] Y. Kalechman, I. Sotnik-Barkai, M. Albeck, B. Sredni, Cancer Res. 53 (1993) 5962–5969.
[5] A. Silberman, Y. Kalechman, S. Hirsch, Z. Erlich, B. Sredni, A. Albeck, ChemBioChem 17 (2016) 918–927.
[6] R.L.O.R. Cunha, M.E. Urano, J.R. Chagas, P.C. Almeida, C. Bincoletto, I.L.S. Tersariol, J.V. Comasseto, Bioorg. Med. Chem. Lett. 15 (2005) 755–760.
[7] H.L. Seng, E.R.T. Tiekink, Appl. Organomet. Chem. 26 (2012) 655–662.
[8] I.A.S. Pimentel, C. de Siqueira Paladi, S. Katz, W.A. de Souza Judice, R.L.O.R. Cunha, C.L. Barbieri, PLoS One 7 (2012) e48780.
[8] B. Sredni, Semin. Cancer Biol. 22 (2012) 60–69.
[9] G.M. Frei, M. Kremer, K.M. Hanschmann, S. Krause, M. Albeck, B. Sredni, B.S. Schnierle, Br. J. Derm. 158 (2008) 578–586.
[10] Y. Ogra, R. Kobayashi, K. Ishiwata, K.T. Suzuki, J. Inorg. Biochem. 102 (2008) 1507–1513.
[11] J. Ibers, Nat. Chem. 1 (2009) 508.
[12] M.S. Silva, L.H. Andrade, Org. Biomol. Chem. 13 (2015) 5924–5929.
[13] M. Brodsky, S. Yosef, R. Galit, M. Albeck, D.L. Longo, A. Albeck, B. Sredni, J. Iterf. Cytok. Res. 27 (2007) 453–462.
[14] M. Halperin-Sheinfeld, A. Gertler, E. Okun, B. Sredni, H.Y. Cohen, Aging 4 (2012) 436–447.
[15] B. Sredni, T. Tichler, A. Shani, R. Catane, B. Kaufman, G. Strassmann, M. Albeck, Y. Kalechman, J. Natl. Cancer. I 88 (1996) 1276–1284.
[16] S. Yosef, M. Brodsky, B. Sredni, A. Albeck, M. Albeck, ChemMedChem 2 (2007) 1601–1606.
[17] B. Sredni, R.R. Caspi, A. Klein, Y. Danziger, Y. Kalechman, M. BenYa'akov, T. Tamari, F. Shalit, M. Albeck, Nature 330 (1987) 173–176.
[18] M. Albeck, T. Tamari, B. Sredni, Synthesis (1989) 635–636.
[19] H. Rosenblatt-Bin, Y. Kalechman, A. Vonsover, R.H. Xu, J.P. Da, F. Shalit, M. Huberman, A. Klein, G. Strassmann, M. Albeck, B. Sredni, Cell. Immunol. (1998) 12–25.
[20] A. Albeck, H. Weitman, B. Sredni, M. Albeck, Inorg. Chem. (1998) 1704–1712.
[21] E. Okun, T.V. Arumugam, S.C. Tang, M. Gleichmann, M. Albeck, B. Sredni, M.P. Mattson, J. Neurochem. (2007) 1232–1241.
[22] E. Okun, Y. Dikshtein, A. Carmely, H. Saida, G. Frei, B.A. Sela, L. Varshavsky, A. Ofir, E. Levy, M. Albeck, B. Sredni, FEBS J. (2007) 3159–3170.
[23] P. Bhattacharyya, Annu. Rep. Prog. Chem. Sect. A Inorg. Chem. (2005) 117–127.
[24] Y. Kalechman, U. Gafter, T. Weinstein, A. Chagnac, I. Freidkin, A. Tobar, M. Albeck, B. Sredni, J. Biol. Chem. (2004) 24724–24732.
[25] H.-L. Seng, H.L. Seng, E.R.T. Tiekink, Appl. Organomet. Chem. (2012) 655–662.
[26] B. Sredni, R.-H. Xu, M. Albeck, U. Gafter, R. Gal, A. Shani, T. Tichler, J. Shapira, I. Bruderman, R. Catane, B. Kaufman, J.K. Whisnant, K.L. Mettinger, Y. Kalechman, Int. J. Cancer (1996) 97–103.
[27] M. Daniel-Hoffmann, B. Sredni, Y. Nitzan, J. Antimicrob. Chemother. 67 (2012) 2165–2172.
[28] A. Silberman, M. Albeck, B. Sredni, A. Albeck, Inorg. Chem. 55 (2016) 10847–10850.
[29] C.R. Princival, M.V.L.R. Archilha, A.A. Dos Santos, M.P. Franco, A.A.C. Braga, A.F. Rodrigues-Oliveira, T.C. Correra, R.L.O.R. Cunha, J.V. Comasseto, ACS Omega 2 (2017) 4431–4439.
[30] Y. Zhao, D.G. Truhlar, J. Chem. Theory Comput. 7 (2011) 669–676.
[31] M.J. Frisch, G.W. Trucks, H.B. Schlegel, G.E. Scuseria, M.A. Robb, J.R. Cheeseman, G. Scalmani, V. Barone, G.A. Petersson, H. Nakatsuji, M.C.X. Li, A.V. Marenich, J. Bloino, B.G. Janesko, R. Gomperts, B. Mennucci, H.P. Hratchian, J.V. Ortiz, A.F. Izmaylov, J.L. Sonnenberg, D. Williams-Young, F. Ding, F. Lipparini, F. Egidi, J. Goings, B. Peng, A. Petrone, T. Henderson, D. Ranasinghe, V.G. Zakrzewski, J. Gao, N. Rega, G. Zheng, W. Liang, M. Hada, M. Ehara, K. Toyota, R. Fukuda, J. Hasegawa, M. Ishida, T. Nakajima, Y. Honda, O. Kitao, H. Nakai, T. Vreven, K. Throssell, J.J.A. Montgomery, J.E. Peralta, F. Ogliaro, M.J. Bearpark, J.J. Heyd, E.N. Brothers, K.N. Kudin, V.N. Staroverov, T.A. Keith, R. Kobayashi, J. Normand, K. Raghavachari, A.P. Rendell, J.C. Burant, S.S. Iyengar, J. Tomasi, M. Cossi, J.M. Millam, M. Klene, C. Adamo, R. Cammi, J.W. Ochterski, R.L. Martin, K. Morokuma, O. Farkas, J.B. Foresman, D.J. Fox, Gaussian 16, Revision B.01, Gaussian, Inc., Wallingford CT, 2016.
[32] M.P. Vazquez-Tato, A. Mena-Menendez, X. Feas, J.A. Seijas, Int. J. Mol. Sci. 15 (2014) 3287–3298.
[33] D.B. Denney, D.Z. Denney, P.J. Hammond, Y.F. Hsu, J. Am. Chem. Soc. 103 (1981) 2340–2347.
[34] H.E. Gottlieb, S. Hoz, I. Elyyashiv, M. Albeck, Inorg. Chem. 33 (1994) 808–811.
[35] K. Krishnan, R.S. Krishnan, Proc. Indian Acad. Sci. Sect. A 64 (1966) 111–122.
[36] H. Frei, T.-K. Ha, R. Meyer, Hs.H. Günthard, Chem. Phys. 25 (1977) 271–281.
[37] K. Nakamoto, Infrared and Raman Spectra of Inorganic and Coordination Compounds 6th Ed. - Part A: Theory and Applications in Inorganic Chemistry, John Wiley & Sons Inc, Hoboken, 2009, pp. 192–204.
[38] K. Nakamoto, Infrared and Raman Spectra of Inorganic and Coordination Compounds 6th Ed. - Part A: Theory and Applications in Inorganic Chemistry, John Wiley & Sons Inc, Hoboken, 2009, pp. 217–220.
[39] K. Büscher, S. Heuer, Bernt Krebs, Z. Naturforsch. B 36 (1981) 307–312.
[40] A. Kovacs, K.-G. Martinson, R.J.M. Konings, J. Chem. Soc. Dalton Trans. (1997) 1037–1042.
[41] N.N. Greenwood, B.P. Straughan, J. Chem. Soc. A (1966) 962–964.
[42] D.M. Adams, D.M. Morris, J. Chem. Soc. A (1967) 2067–2069.
[43] N.S. Dance, W.R. McWhinnie, J. Chem. Soc. Dalton Trans. (1975) 43–45.
[44] D. Lin-Vien, N.B. Colthup, W.G. Fateley, J.G. Grasselli, The Handbook of Infrared and Raman Characteristic Frequencies of Organic Molecules, Academic Press Ltd., San Diego (CA), 1991, pp. 9–28.
[45] A.E. Reed, R.B. Weinstock, F. Weinhold, J. Chem. Phys. 83 (1985) 735–746.
[46] B. Fresch, H.G. Boyen, F. Remacle, Nanoscale 4 (2012) 4138–4147.
[47] A.V. Marenich, C.J. Cramer, D.G. Truhlar, J. Phys. Chem. B 113 (2009) 6378–6396.
[48] S.L. Chua, K. Sivakumar, M. Rybtke, M. Yuan, J.B. Andersen, T.E. Nielsen, M. Givskov, T. Tolker-Nielsen, B. Chao, S. Kjelleberg, L. Yang, Sci. Rep. 5 (2014) 10052.
[49] Z.H. Lin, C.H. Lee, H.Y. Yun, H.T. Chang, Chem. Asian J. 7 (2012) 930–934.
[50] E.H. Morales, C.A. Pinto, R. Lurasci, C.M. Munoz-Villagran, F.A. Cornejo, S.W. Simpkins, J. Nelson, F.A. Arenas, J.S. Piotrowski, C.L. Myers, H. Mori, C.C. Vasquez, Nat. Commun. 8 (2017) 15320.
[51] R.C. Molina-Quiroz, C.M. Munoz-Villagran, E. de la Torre, J.C. Tantalean, C.C. Vasquez, J.M. Perez-Donoso, PLoS One 7 (2012) e35452.